

# Portable high energy gamma ray imagers<sup>1</sup>

S.V. Guru<sup>a,\*</sup>, Z. He<sup>a</sup>, D.K. Wehe<sup>a</sup>, G.F. Knoll<sup>a</sup>, R.H. Redus<sup>b</sup>, M.R. Squillante<sup>b</sup>

<sup>a</sup>Department of Nuclear Engineering, The University of Michigan, Ann Arbor, MI 48109, USA

<sup>b</sup>Radiation Monitoring Devices, Watertown, MA 02172, USA

Received 6 February 1996

## Abstract

To satisfy the needs of high energy gamma ray imagers for industrial nuclear imaging applications, three high energy gamma cameras are presented. The RMD-Pinhole camera uses a lead pinhole collimator and a segmented BGO detector viewed by a 3 in. square position sensitive photomultiplier tube (PSPMT). This pinhole gamma camera displayed an energy resolution of 25.0% FWHM at the center of the camera at 662 keV and an angular resolution of 6.2° FWHM at 412 keV. The fixed multiple hole collimated camera (FMCC), used a multiple hole collimator and a continuous slab of NaI(Tl) detector viewed by the same PSPMT. The FMCC displayed an energy resolution of 12.4% FWHM at 662 keV at the center of the camera and an angular resolution of 6.0° FWHM at 412 keV. The rotating multiple hole collimated camera (RMCC) used a 180° antisymmetric rotation modulation collimator and CsI(Tl) detectors coupled to PIN silicon photodiodes. The RMCC displayed an energy resolution of 7.1% FWHM at 662 keV and an angular resolution of 4.0° FWHM at 810 keV. The performance of these imagers is discussed in this paper.

## 1. Introduction

A first generation raster scanning gamma camera was constructed at the University of Michigan in 1991 [1]. While demonstrating good spatial and energy resolution, this camera required very lengthy data acquisition times. The set of mechanically collimated imagers discussed here was built to reduce the data acquisition time while retaining the spatial and energy resolution of the first generation raster scanning camera.

Mechanically collimated gamma ray imaging involves a four-step procedure: mechanically limiting the direction of incoming gamma rays, detecting these gamma rays, collecting the energy and spatial information about the detected event from the gamma ray detector, and processing this data to produce a two-dimensional map of the distribution of radioactivity at the source plane.

### 1.1. Directionality of the gamma rays

The directionality of the gamma rays can be determined

using mechanical collimators<sup>2</sup>. A singular aperture drilled in a block of lead can provide sufficient information on the directionality of the gamma rays for imaging [1]. Pinhole collimators and multiple hole collimators have been used in nuclear medicine to image radioactivity distributions [4,5]. Unlike some multiple hole collimators, approximations to pinholes can be easily fabricated and can yield good results at low ( $\leq 100$  keV) energies. Coded apertures, which share the advantage of multiple openings and large field of views, have been used in gamma ray astronomy [6–8]. Fig. 1 shows these collimators and their respective advantages and disadvantages.

### 1.2. Gamma ray detection

Gamma ray detection is typically achieved using scintillator materials such as NaI(Tl), CsI(Tl), CsI(Na) or BGO for applications where their lower cost, absence of required cooling, radiation hardness and moderate energy resolution are factors. CsI(Tl) has the highest yield and its wavelength of maximum emission matches the spectral response of commonly used photodiodes. NaI(Tl) has the highest light yield among the scintillators whose wave-

<sup>1</sup> This work was supported under the US Department of Energy, Robotics for Hazardous Environments, Grant No. DOE-FG02-86NE37969.

\* Corresponding author. Currently with GE Corporate Research & Development, Schenectady, NY 12301, USA. E-mail: guru@umich.edu.

<sup>2</sup> The direction of the gamma rays can also be determined by means of electronic collimation ([2,3]). However, this paper focusses on mechanical collimators.

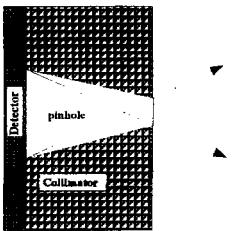
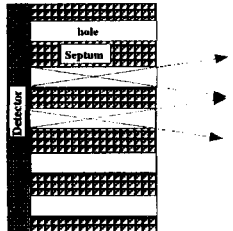
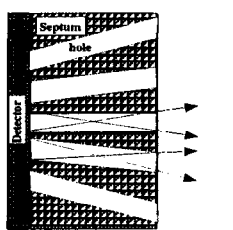
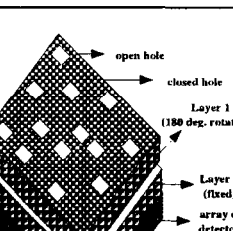
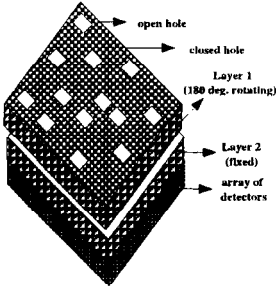
Type of mechanical collimator		Advantages	Disadvantages
Pinhole collimator		<ol style="list-style-type: none"> <li>1. Simple to fabricate</li> <li>2. Large field of view possible</li> </ol>	<ol style="list-style-type: none"> <li>1. Subtends small solid angle relative to source</li> <li>2. Concept of pinhole deteriorates at higher energy of the incident gamma rays due to penetration</li> </ol>
Multiple hole collimators		<ol style="list-style-type: none"> <li>1. Simple to fabricate</li> <li>2. Greater stopping power than the pinhole collimator</li> <li>3. Multiple openings</li> </ol>	<ol style="list-style-type: none"> <li>1. Fields of view from the neighbouring holes overlap beyond some source distance</li> <li>2. Dead areas not seen for relatively small source distances</li> </ol>
Parallel hole, parallel collimator		<ol style="list-style-type: none"> <li>1. Multiple openings</li> <li>2. Each opening with large field of view possible</li> <li>3. Minimal septal penetration for high energy gamma imaging</li> </ol>	<ol style="list-style-type: none"> <li>1. Depending upon the source-collimator distance, might need camera motion to sample the entire source plane.</li> <li>2. More complex to fabricate than options above</li> <li>3. Multiple aperture reconstruction scheme for best resolution</li> </ol>
Parallel hole, diverging collimator		<ol style="list-style-type: none"> <li>1. Multiple openings</li> <li>2. Each opening with large field of view possible</li> <li>3. Minimize septal penetration for high energy gamma imaging</li> <li>4. Good for background rejection</li> </ol>	<ol style="list-style-type: none"> <li>1. More complicated reconstruction scheme</li> <li>2. More complex to fabricate than options above</li> <li>3. Requires two measurements for each image</li> </ol>
Rotation modulation antisymmetric collimator		<ol style="list-style-type: none"> <li>1. Multiple openings</li> <li>2. Each opening with large field of view possible</li> <li>3. Minimize septal penetration for high energy gamma imaging</li> <li>4. Good for background rejection</li> </ol>	<ol style="list-style-type: none"> <li>1. More complicated reconstruction scheme</li> <li>2. More complex to fabricate than options above</li> <li>3. Requires two measurements for each image</li> </ol>

Fig. 1. Mechanical collimators considered for the imagers.

length of maximum emission matches the spectral response of the bialkali photocathode used in most photomultiplier tubes, while BGO has the highest stopping power [9]. Semiconductor detectors such as Si, HPGe, CdZnTe [3,10–13] have been used in gamma ray imagers, but are not considered for our applications due to the factors mentioned above. Other promising materials, such as YAP, YAG, LSO and GSO were not chosen due to their cost and availability. Due to their high light yield and ruggedness, NaI(Tl) was chosen as the scintillator to be used with PSPMT while CsI(Tl) was chosen as the scintillator to be

used with photodiodes. The optical Monte Carlo code DETECT [14] was used to determine the dimensions and face treatment of these scintillators.

### 1.3. Light collection

The readout from scintillation detectors has traditionally been accomplished by photomultiplier tubes (PMT). In the standard gamma camera [4], an array of PMTs is used to provide the 2D distribution of scintillation events on the detector plane. With the advent of the PSPMT technology

[15], a single PSPMT performs the role of an array of PMTs, thus significantly reducing the hardware and software requirements of a gamma camera [16–20]. The PSPMT produces four outputs  $X_1$ ,  $X_2$ ,  $Y_1$  and  $Y_2$  from its anode resistive chains along the  $X$  and  $Y$  directions. Spatial coordinates of the interaction position are calculated using

$$X = (X_1 - X_2)/(X_1 + X_2), \quad (1)$$

$$Y = (Y_1 - Y_2)/(Y_1 + Y_2). \quad (2)$$

The energy deposited by a scintillation event ( $E$ ) is determined from the sum of the four outputs and is given by

$$E \propto X_1 + X_2 + Y_1 + Y_2. \quad (3)$$

When using CsI(Tl) detectors, due to the better match of the emission spectrum of the CsI(Tl) detector with the absorption spectrum of a Si photodiode, an array of photodiodes (PD) is used to collect the light generated within the scintillator [21].

#### 1.4. Data processing

The four outputs of the PSPMT are sampled and digitized. Using Eqs. (1)–(3), the values of  $X$ ,  $Y$  and  $E$  are calculated. These digital values are used to construct the two-dimensional radioactivity distribution and the measured energy spectrum at the source plane. A sampling and peak determination circuit was designed and operated with an analog devices RTI-860 ADC [22]. Data acquisition and image display software was developed using the C++ language. A commercial board, PSPMT interface board, was fabricated by radiation monitoring devices (RMD) [23] to perform the sampling and peak determination. The PSPMT interface board was used with a Metrabyte DAS-16 ADC in the RMD-Pinhole camera. The PSPMT interface software performs the data acquisition and image display. The PSPMT interface software also gives the ability to perform corrections to the gain variations across the photocathode of the PSPMT. The PSPMT photocathode gain varies non-intuitively across the face of the PSPMT. A map of the gain across the photocathode was generated by uniformly illuminating the detector mounted on the PSPMT with monoenergetic gamma rays. The relative location of the photopeaks at various positions on the photocathode gives a measure of the relative variation in the gain of the photocathode. This calibration is saved and used to perform an energy correction.

## 2. RMD-Pinhole gamma camera

The RMD-Pinhole camera was fabricated by RMD using a pinhole collimator, a segmented BGO detector and a PSPMT [24], as shown in Fig. 2. A pinhole collimator was fabricated out of a 5 cm thick lead block with a

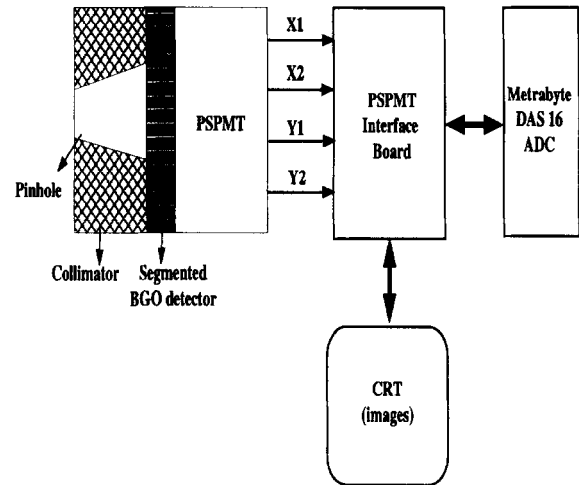


Fig. 2. Schematic of the RMD-Pinhole camera.

frustum shaped hole drilled in it. The base of the hole is 2.6 cm in diameter and faces the detector. The aperture facing the source distribution is 0.3 cm in diameter, thus giving the pinhole a total opening angle of  $31^\circ$ . The BGO detector is segmented, with each voxel measuring  $2.5 \text{ mm} \times 2.5 \text{ mm} \times 1.0 \text{ cm}$ . The spacings between the segments are coated with a layer of an optical reflector (magnesium oxide) which minimizes the optical cross talk between neighbouring segments of the scintillator, but does not prevent the gamma cross talk between them. These scintillation events within the BGO detectors are converted to electrical pulses using the Hamamatsu R-2487-05 position sensitive photomultiplier tube (PSPMT).

The four output signals from the PSPMT ( $X_1$ ,  $X_2$ ,  $Y_1$  and  $Y_2$ ) are passed to a PSPMT interface board. The interface board sums the four signals to give the total energy ( $E$ ) deposited by the gamma ray and performs the charge division to yield the interaction position ( $X$  and  $Y$ ). The PSPMT interface software is used to construct a two-dimensional map of the interaction positions. The position information from gamma rays having multiple interactions in the crystal only contribute to noise, and hence an energy window is set on the PSPMT interface board to reject most of the scattered events. The gain variations across the PSPMT face account for pulse height differences up to a factor of 2 [25]. Hence a calibration is performed to map the positional dependence of the gain variation, which is subsequently used as a uniformity correction. Unlike coded apertures, for a true pinhole collimator there is a direct correspondence between the position of a single event on the detector plane and the incident gamma ray position on the source plane. This implies that the raw accumulating data directly reflects the (inverted) source plane distribution, which is an advantage when imaging unknown sources. Furthermore, the magnification of the camera can be adjusted by varying the ratio of the collimator–detector distance.

An upgraded version of this RMD-Pinhole gamma camera using a tungsten pinhole collimator is presented in Ref. [26].

### 2.1. Energy resolution

The energy resolution for this camera was measured at its center, which was covered by one voxel ( $2.5\text{ mm} \times 2.5\text{ mm} \times 1.0\text{ cm}$ ) and yielded an energy resolution of 25.0% FWHM at 662 keV. For comparison, an earlier imager using a  $1.25\text{ cm} \times 1.25\text{ cm}$  right circular cylinder of BGO displayed an energy resolution of 12.9% FWHM at the same energy. The cause of the poor resolution for the segmented BGO was not investigated. However, the PSPMT was not a contributor to the degraded energy resolution.

### 2.2. Angular resolution

In the RMD-Pinhole gamma camera a segmented slab of BGO is used to restrict the visible photons that are produced to the pixel in which they are formed. Since the pixels are coated with an optically reflecting layer of MgO, photons generated within a segment are distributed uniformly over the entire area of the photocathode covered by that segment. The point of interaction of the gamma ray is determined by the centroid calculations performed by the PSPMT. An event taking place within a segment is always located at the center of the segment and it is not possible to detect events within a segment of the scintillator. Hence the size of the segment ( $2.5\text{ mm} \times 2.5\text{ mm}$ ) is the limiting factor to the spatial resolution of the crystal. The limiting PSPMT spatial resolution using the hardware centroid method has been measured to be 0.5 mm and is thus not the limiting factor in determining the spatial resolution. From a cross section of the image obtained from the RMD-Pinhole camera (such as Fig. 3) angular resolution of the pinhole camera was measured to be  $6.2^\circ$  FWHM at 412 keV [27].

### 2.3. Imaging results

Fig. 3 is an image of an M-shaped activated gold wire ( $^{198}\text{Au}$ ), emitting gamma rays of 412 keV. The source activity was  $100\ \mu\text{Ci}$  and was located 25 cm away from the pinhole and the acquisition was 3 min.

As seen in Fig. 3, the pinhole gamma camera worked well for lower energy gamma rays, such as 412 keV. However, with increasing incident gamma ray energy, the ability of the pinhole to form an image decreases and hence leads to a degraded image quality. As a result, the hardware and software simplicity make the pinhole a more viable option for relatively lower energy ( $\leq 500\text{ keV}$ ) gamma rays.



Fig. 3. Image of a M shaped  $^{198}\text{Au}$  wire, obtained with the RMD-Pinhole camera.

## 3. Fixed multiple hole collimated camera (FMCC)

The FMCC high energy gamma ray imager was constructed using a multihole collimator, a continuous slab of NaI(Tl) detector and a PSPMT [28] as shown in Fig. 4. A  $5 \times 5$  multiple hole tungsten collimator was fabricated from a 2.54 cm thick block of tungsten with hole diameters of 0.20 cm and a minimum septal thickness of 0.63 cm. The slant angle of the holes was chosen to be  $10^\circ$  to ensure that, neglecting septal penetration, the fields of view from each of the holes will overlap at infinity. However, for higher energy incident gamma rays, septal penetration causes this effective distance to decrease as discussed in eq. [29]. From the DEFECT modeling, a continuous slab of NaI(Tl) detector measuring  $7.5\text{ cm} \times 7.5\text{ cm} \times 1.0\text{ cm}$  was chosen. The inner faces of the scintillator was coated with a light absorbing layer on all faces, with the exception

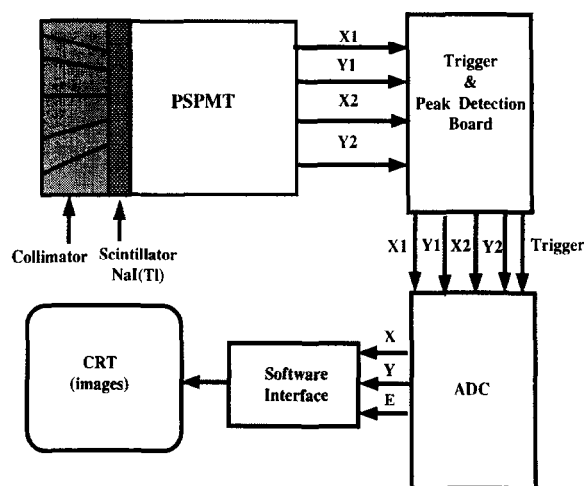


Fig. 4. Schematic of the FMCC.

of the exit face. This coating reduces the number of photons detected which was reflected off the crystal faces and distort the measured position of the gamma interaction. DETECT modeling indicated that a dark coating on the crystal sides would reduce the systematic error associated with determining the centroid of the light output near the edges, and thus increase the available field of view of the camera. However, the dark coating does lead to reduced energy and spatial resolution of the imager. The advantage of the larger field of view was of greater importance to this application and hence the scintillator was coated with an absorbing rather than reflecting layer [27]. This tradeoff is discussed in more detail in a forthcoming paper.

The scintillation events within the NaI(Tl) slab are detected by the Hamamatsu R-2487-05-PSPMT. A peak sample and hold board was fabricated and used in conjunction with the multi-channel ADC (analog devices RT-860) to record the peak values from the four output signals of the PSPMT [22]. Since our electronics is similar in functionality to the PSPMT interface board described in Section 2, a decision was made to use the RMD commercially available PSPMT interface board. Hence, the RMD-Pinhole camera and the FMCC used the same PSPMT interface board and corresponding software to acquire the data and display the images.

### 3.1. Energy resolution

Since the multihole gamma camera uses a single slab of NaI(Tl), we expect better energy resolution than for the pinhole camera with its segmented BGO detector. However, this gain is somewhat offset by the photons which are lost to the light absorbing layer coated on the five inner faces of this crystal and leads to a measured energy resolution of only 12.4% FWHM at 662 keV at the center of the camera. The measured energy resolution varies from 12 to 20% FWHM for 662 keV and from 17 to 23% for 122 keV across the crystal. The variation in the energy resolution is due to the gain variation across the photocathode of the PSPMT, coupled with the light spread in the crystal.

### 3.2. Angular resolution

The spatial resolution of the NaI(Tl) detector mounted on the PSPMT was measured to be 2.9 mm at 122 keV and 5.0 mm at 662 keV [28]. Due to the continuous nature of the crystal and its 1.0 cm thickness, scattered events dominate at higher energies leading to a degradation in the spatial resolution of the crystal. The multiple hole collimator used in this camera has an opening angle of 5° FWHM. From the cross-sectional data of an image (such as Fig. 6), the overall angular resolution of the FMCC was measured to be 6° FWHM at 412 keV [27].

### 3.3. Imaging results

For relatively small source–camera distances, there are areas on the source plane that are not mapped onto the scintillator, leading to blind spots in the image. Fig. 5 shows the shadow of the collimator projected on to the image of the  $^{198}\text{Au}$  ‘‘M’’ source. This problem is overcome by panning and tilting the camera to ensure a complete sampling of the source plane. With the knowledge of the orientation of the camera at each of these positions and the source–detector distance, the data from the multiple images is integrated to form the distribution of radioactivity on the source plane. The data integration method is described in Ref. [30].

Fig. 6 is an image of a 100  $\mu\text{Ci}$  ‘‘U’’ shaped, activated gold wire located 10 cm away from the multihole gamma camera. The amount of tilting and panning was determined from the known source distance. The multihole camera was panned and tilted to image in  $5 \times 5$  directions, generating 25 raw images of the source distribution at each of these directions. The data from these 25 images were integrated using the multiple aperture integration technique [30] to yield the image of the source distribution shown in Fig. 6. The final image shown in Fig. 6 was obtained in 10 min and correctly identifies the distributed radiation present within its field of view. The light shadows seen on the vertical legs in Fig. 6 are probably due to the response of the neighboring holes, since the point source response function shows minor side lobes for neighboring holes [27]. These points have an intensity  $\approx 10\%$  of the actual points and would disappear under a thresholding operation. A more rigorous reconstruction which accounted for the PSRF would likely reduce these shadows as well.



Fig. 5. A typical gamma ray image of a continuous M shaped source distribution of  $^{198}\text{Au}$  (412 keV), as seen on the detector plane of the FMCC. This image shows the shadow of the collimator expected from a single snap shot of the source plane located 10 cm away.

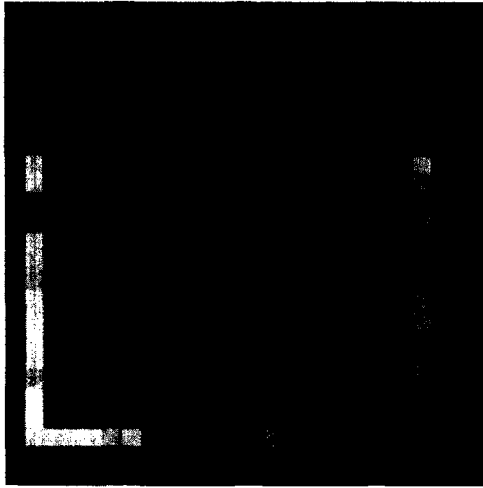


Fig. 6. Integrated image (25 × 25) of a U shaped  $^{198}\text{Au}$  (412 keV) wire, located 10 cm away from the FMCC.

### 3.4. Sensitivity of FMCC

The sensitivity of the camera,  $\xi$ , can be described as the minimum activity required for a source to be detected significantly above the noise level of the camera. This is defined as the signal to noise ratio.

$$\xi = \frac{N_{\text{source+bkg}} - N_{\text{bkg}}}{\sqrt{N_{\text{bkg}}}} \quad (4)$$

where  $\xi$  is the sensitivity,  $N_{\text{source+bkg}}$  is the total counts registered by the camera with a source present and  $N_{\text{bkg}}$  is the background registered by the camera. Both the source and the background are counted for the same duration.  $\xi$  is the size of the measured total signal above the measured background counts in units of the standard deviation of the background counts. Using a 25  $\mu\text{Ci}$  gold point source (412 keV) located 50 cm away from the camera along the central axis of the camera and a counting time of 5000 s, the signal to noise ratio ( $\xi$ ) of the image was measured to be 121 for the 544 background counts observed. This sensitivity measurement was made for a single image. If we define “detection” as  $\xi = 3$  the camera will “detect” a 23  $\mu\text{Ci}$  source of 412 keV located at a distance of 1 m in 1 min in the same background. This experimentally measured value of the sensitivity is in agreement with the theoretical value predicted during the design phase.

## 4. Rotating multiple hole collimated camera (RMCC)

The rotating multiple hole collimated camera (RMCC), was constructed using an antisymmetric rotation modulation collimator and an array of CsI(Tl) detectors coupled to silicon PIN photodiodes.

To extend the upper energy limit of our imagers further

into the MeV range and to improve the signal to noise ratio of the images, an antisymmetric rotation modulation collimator was constructed. This collimator consists of two layers of multiple hole collimators. The holes in the top layer of the multiple hole collimators are arranged in a 180° antisymmetric manner. By rotating this layer by 180°, all the detectors that had viewed an open aperture would be aligned to a septum. Thus a measure of the signal and the background is achieved in two measurements taken at the same orientation of the camera.

This camera is designed to use a 4 × 4 array of 1.0 cm × 1.0 cm × 3.0 cm CsI(Tl) detectors coupled to a 1.0 cm square silicon PIN photodiode, Hamamatsu S3590-03. An AMPTEK A 250 charge-sensitive preamplifier and an ORTEC 572 shaping amplifier were also used. The resultant signals were digitized using an analog devices ADC RT-860. In the initial prototype fabricated, a single detector assembly was used to permit quick design modifications. The presence of the entire array was simulated by placing the imager on a pan and tilt table. The control of the ADC, motors for the pan and tilt table and the data manipulation and imaging software was done on a 486 PC. The schematic of this prototype is shown in Fig. 7.

### 4.1. Energy resolution

An energy resolution of 7.1% FWHM at 662 keV was measured with this antisymmetric gamma camera. As

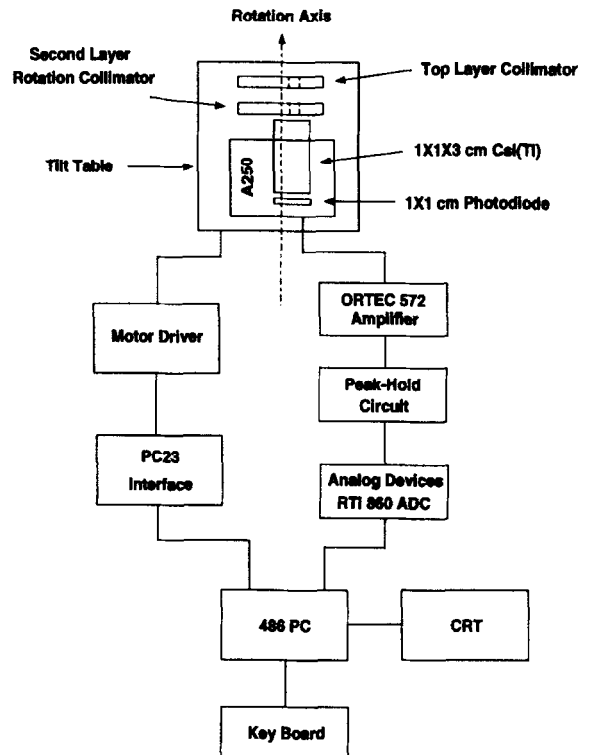


Fig. 7. Schematic of the RMCC.

expected, the 3.0 cm long crystal of CsI(Tl) gave the best energy resolution measured among the three imagers discussed here. The discrete nature of the CsI(Tl) detectors allows the use of a longer crystal, ensuring a greater interaction efficiency for the gamma rays.

#### 4.2. Angular resolution

The multiple hole antisymmetric collimator has an angular resolutions of  $4^\circ$  FWHM at 810 keV. The maximum likelihood estimation method (MLEM) using the measured PSRF of the camera enhanced the spatial resolution of the imager to  $2^\circ$  FWHM at 810 keV [21].

#### 4.3. Imaging results

Fig. 8 is an image of a 1 mCi  $^{58}\text{Ni}$  U shaped activated nickel wire (810 keV) located 1 m away from the imager and taken over 6 h. The presence of a full detector array was simulated by panning and tilting the single detector module. With the presence of an  $N \times N$  array of detectors, the data acquisition time should be reduced by a factor of  $N^2$ .

The antisymmetric gamma camera demonstrates good imaging ability at higher energies due to the rotating collimator design and the discrete long crystals used in this camera. The cost of this device and its complexity increase when an array of detectors, each with its own silicon PIN photodiode and readout electronics, is used instead of the

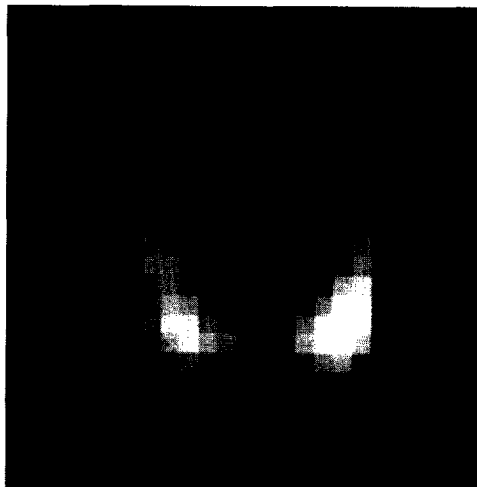


Fig. 8. Image of a U shaped  $^{58}\text{Ni}$  wire, obtained with the RMCC.

single detector module used in the prototype. The data from this imager also needs to be post-processed, unlike the pinhole gamma camera.

#### 4.4. Sensitivity of RMCC

As defined earlier for the FMCC, the sensitivity of the camera is described as the amount of activity that will significantly be detected over a preset noise level by the camera. A  $10 \mu\text{Ci}$  point  $^{137}\text{Cs}$  source (662 keV) was

Table 1  
Measured performance parameters of the imagers described in the text

Parameter	Raster scanner [1]	RMD-Pinhole [24]	FMCC [29]	RMCC [21]
1 <b>Detector</b>	BGO + PMT	BGO + PSPMT	NaI (Tl) + PSPMT	CsI(Tl) + PD
Configuration:	single detector	segmented detector	a slab of detector	array of detectors
Dimensions:	1.25 × 1.25 cm	2.5 × 2.5 × 10.0 mm	7.5 × 7.5 × 1.0 cm	1.5 × 1.5 × 3.0 cm
2 <b>Collimator</b>	single aperture	pinhole	multiple hole	multiple hole (180° anti-symmetric)
Material:	Lead	Lead	Tungsten	Lead, two layers
no. of apertures:	1	1	5 × 5	5 × 5 (tested with a 1 × 1)
Absolute Efficiency: (1 MeV of 1 m)	≈ 10 <sup>-6</sup>	≈ 10 <sup>-6</sup>	≈ 10 <sup>-6</sup>	≈ 10 <sup>-6</sup>
3 <b>Energy resolution</b> (at 662 keV)	12.9% FWHM	25.0% FWHM	12.4% FWHM	7.1% FWHM
4 <b>Angular resolution</b> (at 662 keV)	2.5°	6.2° (at 412 keV)	6.0° (at 412 keV)	4.0°
5 <b>Sensitivity</b>	N/A	N/A	23 μCi (at 412 keV)	20 μCi (at 662 keV)
Activity that can be detected 3σ above the background in 1 min at a distance of 1 m (measured along the axis)				
Post processing required?	Yes	No	Yes	Yes
Processing time:	~minutes	Real-time	~minutes	~minutes

located 1 m away from the camera. The camera was panned and tilted in steps of  $1.5^\circ$  over a field of view of  $12^\circ \times 12^\circ$ . This resultant image had a signal to noise ratio of 12. From these numbers and using Eq. (4), we can extrapolate that RMCC is sensitive enough to detect a  $0.5 \text{ mCi } ^{137}\text{Cs}$  source located 5 m away with a  $3\sigma$  confidence level in about 1 min.

## 5. Conclusions

A set of portable high energy imagers has been designed and tested. The performance of the various imagers is summarized in Table 1. The results demonstrate the feasibility of imaging high energy (0.5–2 MeV) gamma rays. Given a set of imaging conditions, these results should aid in the selection of a particular camera design. Gamma ray imaging is currently unavailable to the nuclear industry and we are currently field-testing these devices to demonstrate their applicability in practical environments.

## References

- [1] T.A. DeVol, D.K. Wehe and G.F. Knoll, Nucl. Instr. and Meth. A 299 (1990) 495.
- [2] M. Singh, Med. Phys. 10 (1983) 421.
- [3] J.B. Martin, N. Dogan, J.E. Gormley, G.F. Knoll, M. O'Donnell and D.K. Wehe, IEEE Trans. Nucl. Sci. NS-41 (1994) 1019.
- [4] H.O. Anger, Rev. Sci. Instr. 29 (1958) 27.
- [5] H.O. Anger, J. Nucl. Med. 5 (1964) 515.
- [6] E.E. Fenimore and T.M. Cannon, Appl. Opt. 17 (1978) 337.
- [7] E.E. Fenimore, Appl. Opt. 17 (1978) 3562.
- [8] J.S. Fleming and B.A. Goddard, Nucl. Instr. and Meth. 221 (1984) 242.
- [9] G.F. Knoll, Radiation Measurements, 2nd ed. (Wiley, 1988).
- [10] J.F. Butler et al., Phys. Med. Imaging 1896 (1993) 30.
- [11] F.P. Doty et al., Nucl. Instr. and Meth. A 353 (1994) 356.
- [12] R. Polichar, R. Schirato and J. Reed, Nucl. Instr. and Meth. A 353 (1994) 349.
- [13] I. Fujieda, S. Nelson, R.A. Street and R.L. Weisfield, Mater. Res. Soc. Symp. Proc. 219 (1991) p. 537.
- [14] G.F. Knoll, T.F. Knoll and T.M. Henderson, IEEE Trans. Nucl. Sci. NS-35 (1988) 872.
- [15] H. Kume and S. Muramatsu, IEEE Trans. Nucl. Sci. NS-33 (1986) 359.
- [16] N.J. Yasillo, R.N. Beck and M. Cooper, IEEE Trans. Nucl. Sci. NS-37 (1990) 609.
- [17] Z. He, A.J. Bird, D. Ramsden and Y. Meng, IEEE Trans. Nucl. Sci. NS-40 (1993) 447.
- [18] T.D. Milster et al., J. Nucl. Med. 31 (1990) 632.
- [19] N.J. Yasillo et al., A single tube miniature gamma camera. Conf. Record IEEE NSS/MIC (1993).
- [20] C.E. Ordenez et al., Simulation of imaging with NaI(Tl) crystals and position sensitive photomultiplier tubes. Conf. Record, IEEE NSS/MIC (1993).
- [21] Z. He, S.V. Guru, D.K. Wehe, G.F. Knoll, A. Truman and D. Ramsden, IEEE Trans. Nucl. Sci. NS-42 (1995) 668.
- [22] J.C. Ferreria, Professional Engineer, Dissertation, The University of Michigan (1994).
- [23] Radiation Monitoring Devices, Position Sensitive Photomultiplier Interface System, private communication (1993).
- [24] R.H. Redus, M.R. Squillante, J. Gordon, D.K. Wehe and G.F. Knoll, Nucl. Instr. and Meth. A 353 (1994) 324.
- [25] Position-Sensitive Photomultiplier Tubes with crossed wire anodes, R2487 series, Hamamatsu Technical Specification Sheets.
- [26] R. Redus, M. Squillante, G. Entine, P. Bennet, G. Knoll, D. Wehe and S. Guru, An imaging nuclear survey system, presented at 1995 IEEE Nucl. Sci. Symp. (1995).
- [27] S.V. Guru, Ph.D. Dissertation, The University of Michigan (1995).
- [28] S.V. Guru, Z. He, J.C. Ferreria, D.K. Wehe and G.F. Knoll, Nucl. Instr. and Meth. A 353 (1994) 328.
- [29] S.V. Guru, J.D. Valentine, D.K. Wehe and G.F. Knoll, IEEE Trans. Nucl. Sci. NS-41 (1994) 898.
- [30] S.V. Guru, Z. He, D.K. Wehe and G.F. Knoll, IEEE Trans. Nucl. Sci. NS-42 (1995) 940.